CHALMERS
UNIVERSITY OF TECHNOLOGY

Experimental Determination of Heat Transfer Coefficient to Horizontal Tube Submerged in Packed-fluidized Bed

Master's thesis in Sustainable Energy Systems

Pontus Andersson

DEPARTMENT OF SPACE, EARTH AND ENVIRONMENT

CHALMERS UNIVERSITY OF TECHNOLOGY

Gothenburg, Sweden 2020
www.chalmers.se

DEPARTMENT OFSPACE, EARTH AND ENVIRONMENT
CHALMERS UNIVERSITY OF TECHNOLOGY
Gothenburg, Sweden
www.chalmers.se

Experimental Determination of Heat Transfer Coefficient to Horizontal Tube Submerged in Packed-fluidized Bed

Pontus Andersson

CHALMERS
UNIVERSITY OF TECHNOLOGY

Experimental Determination of Heat Transfer Coefficient to Horizontal Tube Submerged in Packed-fluidized bed

PONTUS ANDERSSON

Supervisor: Viktor Stenberg, Department of Space, Earth and Environment

Supervisor: Nasrin Nemati, Department of Space, Earth and Environment

Examiner: Magnus Rydén, Department of Space, Earth and Environment

Master’s Thesis 2020

Department of Space, Earth and Environment

Division of Energy Technology

Chalmers University of Technology

SE-41296 Gothenburg

Telephone: +46 31 772 1000

Experimental Determination of Heat Transfer Coefficient to Horizontal Tube Submerged in Packed-fluidized Bed

PONTUS ANDERSSON

Department of Space, Earth and Environment

Chalmers University of Technology

Abstract

The aim of the thesis was to experimentally determine the heat transfer coefficient to the surface of a horizontal tube submerged in a bubbling fluidized bed containing packing material. This was done for bed temperatures ranging from 400°C to 900°C and superficial gas velocities from 0.04 m/s to 0.411 m/s. Six different packing materials were evaluated; two sizes of aluminium silicate balls, two sizes of Raschig rings, an RVT metal saddle ring (RMSR) and an RVT Hiflow® ring. Additionally, the pressure drop of the packed fluidized beds was measured. Using the pressure data, the vertical segregation of the packed fluidized beds was also estimated.

The experimental work was carried out in a lab-scale reactor. The determination of the bed-to-tube heat transfer coefficient was done by measuring the increase in temperature of water flowing through a horizontal tube submerged in the packed bed. An electrical furnace provided the heat to the reactor. Air was used as a fluidizing gas and the bed particles consisted of Baskarp B-28 silica sand, sieved to a size of 212-300 μm.

The bed-to-tube heat transfer coefficient increased with increasing bed temperature for all evaluated packing materials. In general, the packed-fluidized bed cases showed lower heat transfer coefficients than a reference case of a fluidized bed containing no packing material. The RMSR saddle ring performed the best, with a maximum heat transfer coefficient of 1298 W/(m^{2}K), only slightly lower than the reference case. The Hiflow ring, despite its similarities to the RSMR ring, performed approximately 25% worse at temperatures of 800°C or higher, at fully fluidized conditions.

For all packings, the heat transfer coefficient increased with increasing gas velocity up to a certain maximum value, after which it decreased slowly with increasing gas velocity. Also, for all packings, the heat transfer coefficient was lower than the heat transfer coefficient of the fluidized bed when it contained no packing material. The exception being the RMSR packing at high velocities.

Important packing material parameters for limited negative effect on the heat transfer ability and pressure drop of the bed were high packing void ratio, open packing structure and the packing not physically covering heat exchange surfaces to a great degree.

The best performing packing, which had the least impact on bed heat transfer and pressure drop, was the RMSR 25-3.

Keywords: Confined fluidization, packed fluidized bed, heat transfer

Acknowledgement

Firstly, I would like to give my thanks to my supervisor, PhD student Viktor Stenberg, for his support and guidance during the production of this thesis. My thanks are also extended to my supervisor, PhD student Nasrin Nemati, whose assistance and input was invaluable during the experimental part of the thesis. Likewise, I would like to extend my gratitude to my examiner, Associate Professor Magnus Rydén, for his support and guidance. Finally, I would like to thank Rustan Hvitt and Jessica Bohwalli for their assistance with the practical part of the experimental work.

Pontus Andersson, Gothenburg, January 2019

Table of Contents

List of Figures

List of Tables

Nomenclature

A_i	Tube inner surface area	m^2
A_o	Tube outer surface area	m^2
$c_{P,water}$	Heat capacity of water	J/(kgK)
d_i	Inner tube diameter	m
d_o	Outer tube diameter	m
H	Height of the fluidized bed	m
h_i	Heat transfer coefficient from tube wall to water flow	$W/(m^2K)$
h_o	Heat transfer coefficient from bed to tube	$W/(m^2K)$
j_H	Tube inside heat transfer factor	
k_{wall}	Tube wall thermal conductivity	W/(mK)
k_{water}	Water thermal conductivity	W/(mK)
$m_{bp,pack}$	Mass of bed particles in packing region	kg
$m_{bp,top}$	Mass of bed particles in top region	kg
$m_{bp,tot}$	Total mass of bed particles	kg
Q	Heat transferred through tube wall	W
T_{bed}	Bed temperature	K or ^oC
$T_{wall,avg}$	Average temperature of wall	K or ^oC
$T_{wall,in}$	Temperature of inside of tube wall	K or ^oC
$T_{wall,out}$	Temperature of outside of tube wall	K or ^oC
$T_{water,avg}$	Average water temperature inside tube	K or ^oC
$T_{water,in}$	Inlet water temperature	K or ^oC
$T_{water,out}$	Outlet water temperature	K or ^oC
U_o	Overall heat transfer coefficient	$W/(m^2K)$
u_{mf}	Minimum fluidization velocity	m/s
u_t	Terminal velocity	m/s
u_{water}	Water velocity inside tube	m/s
u_0	Fluidization velocity	m/s
$\dot{V}$	Water flow rate	m^3/s

Greek letters

ΔP_{bed}	Pressure drop over the fluidized bed	Pa
ΔP_{packed_region}	Pressure drop over the packed region of the bed	Pa
ΔP_{top}	Pressure drop over the top region of the bed	Pa
ΔT_{LM}	Logarithmic mean temperature	K or ^{o}C
ΔT_{in}	Inlet side temperature difference	K or ^{o}C
ΔT_{out}	Outlet side temperature difference	K or ^{o}C
ε_{bed}	Void fraction of fluidized bed	
ε_{bp}	Fixed bed void fraction of bed particles	
$\varepsilon_{bp,packing}$	Packing interstice volume void fraction	
ρ_s	Density of fluidizing bed material	kg/m^3
ρ_g	Density of fluidizing gas	kg/m^3
ρ_{water}	Density of water	kg/m^3

Dimensionless numbers

Pr	Prandtl number
Re	Reynolds number

1 Introduction

The issue of climate change, brought on by the emission of greenhouse gases, is a major challenge for society at present. To comply with the goals set by international agreements to limit the global average temperature increase, widespread employment of new technologies with a low climate impact is necessary. A promising option is what is commonly referred to as carbon capture and storage, where after the combustion of a fuel the resulting CO_2 is collected. The CO_2 is then stored in a suitable long-term location, examples being aquifers, used oil and gas fields, and deep-sea storages [1,2]. The most problematic issue with carbon capture and storage comes from the need to separate the CO_2 from other gases it might be mixed with, that do not have any impact on the climate. The most attractive source of CO_2, in terms of volume, is flue gas generated during combustion of solid fuels, which usually only contains 10-15% CO_2. A significant amount of energy is needed to obtain pure CO_2 from such streams. Lyngfelt and Leckner put the amount, for a coal-fired power plant, at one-fifth of the total amount of electricity produced [3].

An alternative to post-combustion CO_2 capture options that require costly and energy consuming gas separation processes is the use of a fluidized bed technology known as chemical-looping combustion [4]. It is conceptually based on using solid oxygen carrier particles as the fluidizing material of the bed, to oxidize gaseous fuels and solid fuel volatiles inside a so-called fuel reactor. The oxygen carrier is then circulated to a second reactor, where it is oxidized by an air stream, before being returned to the fuel reactor. See reactions (1) and (2) for the reactions using a generic oxygen carrying metal, Me, and figure 1 for a basic schematic of a chemical looping combustion setup. In practice, the oxygen carrier can be based on affordable and environmentally benign metal oxides of e.g. Fe or Mn. Also untreated mineral ores that are rich in Fe- or Mn-oxides can be used as oxygen carrier with adequate performance.

$$(2n+m)MeO + C_nH_{2m} \rightarrow (2n+m)Me + mH_2O + nCO_2 \quad (1)$$

$$(2n+m)Me + (2n+m)\frac{1}{2}O_2 \rightarrow (2n+m)MeO \quad (2)$$

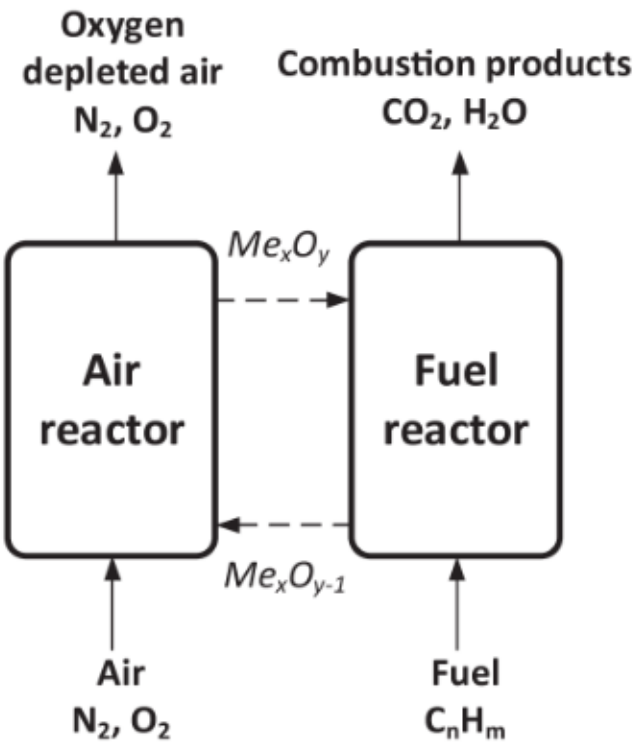

Figure 1: Chemical looping combustion schematic for hydrocarbon fuels [5].

Due to using an oxygen carrier, no nitrogen from the air stream enters the fuel reactor. The resulting flue gas from the fuel reactor mainly consists of CO_2 and water vapour, the latter which can easily be separated by cooling and condensation. A pure stream of carbon dioxide is thus received without the need for costly separation technologies.

Fully developed, a chemical-looping combustion power plant would be physically similar to current circulating-fluidized bed power plants, and most equipment used in the latter would be compatible with Chemical-Looping Combustion. Circulating-fluidized bed plants are currently the default technology choice for biomass combustion and waste incineration at scales over 150 MW_{th} and a competitive choice for lignite and hard coal below 2000 MW_{th}. The chemical-looping combustion concept has been tested in over 50 pilot reactors for a total of over 11000 hours [6].

In chemical-looping combustion, it is desirable for the oxidation of gaseous fuel and solid fuel volatiles in the fuel reactor to be as complete as possible. For reaction (1) to occur, the solid fuel must be gasified and the combustible gases must then come into contact with the oxygen carrier. The gas-solid mass transfer between the fuel gas and bed particle solids occurs at the boundary between the phases, at the surface of the gas bubbles. In many instances, this mass transfer rate could be the step limiting the overall reaction rate. An issue for fluidized beds in general is that the gas bubbles coalesce and grow in size as they rise through the bed. In large-scale reactors, which potentially would need to utilize unusually deep beds, the bubbles are expected to grow to very large sizes [7]. As the size of the bubbles increases, the total amount of bubble surface area in the bed decreases. This leads to an overall decrease in the available mass transfer area between the fuel gas and oxygen-carrying bed particles and the rate of the gas-solid reaction decreases. This is one of the major concerns, when considering scaleup of chemical-looping combustion from where it is today i.e. large lab scale (100-1000 kW_{th}) to demonstration scale (10-50 MW_{th}) and further to full utility scale (100-2000 MW_{th}).

To eliminate bubble growth, the introduction of a packing material into the fluidized bed has been suggested [8]. The material, being of a significantly larger size than the bed particles, would physically limit the maximum growth size of the bubbles as they rise through the voids of the packings, while still allowing for fluidization to occur inside the packing voids.

When a packing material is added to the bed, the movement of the bed particles becomes restricted due to the constricted pathways between the packings. As the bed particles are able to transport heat by their movement through the bed, their restricted movement will lead to a decrease in the heat transported both through the bed and through heat exchange surfaces in contact with the bed [7]. Additionally, the packings would also cover parts of any heat exchange surfaces they come into contact with. Covered surfaces would become unavailable for bed particles to exchange heat through, lowering the amount of heat transferred through the heat exchange surfaces.

The heat transfer coefficient between the bed and heat exchanger surfaces is a key design parameter for fluidized bed boilers, since it will govern reactor size and tube wall design. It is also a critical factor when designing convection sections for removing heat and systems to regulate the bed temperature. However, almost no data exists for the heat transfer coefficient between a packed fluidized bed and a heat exchanging wall surface. Investigating the effect of adding different packing materials to a fluidized bed would therefore be of great interest for chemical-looping combustion, as well as a number of other future fluidized bed applications.

1.1 Aim

The aim of this thesis was to experimentally determine the heat transfer coefficient to the surface of a horizontal tube submerged in a bubbling fluidized bed containing packing material, for varying bed temperatures between 400-900^{o}C and varying superficial gas velocities between 0.04-0.411 m/s. Several different packing materials were evaluated, to determine how certain packing material parameters affect the heat transfer ability and the pressure drop of the bed. The vertical segregation of the fluidizing bed material and the packing material was also estimated for varying superficial gas velocities and varying packing materials.

1.2 Limitations

The work was carried out in a laboratory-scale bubbling fluidized bed reactor, with the setup consisting of only one configuration. No variation in equipment size or bed particle material was investigated. The vertical position of the horizontal tube was not changed. No fuel was added to the reactor and it was heated externally by an electrical furnace. The bed was fluidized with air.

The tube-to-water heat transfer coefficient was determined from correlations. As forced internal convection for fluids in a tube is a common concept, the correlations were assumed to be accurate. The thermal conductivity data for the tube, made of Inconel alloy 600, was sourced from a vendor. Fouling of heat exchange areas was neglected.

The packing materials used in the study were limited to two sizes of aluminium silicate balls, two sizes of Raschig rings, an RVT saddle ring and an RVT Hiflow® ring. The only bed material used was Barskarp fine silica sand.

2 Theory

2.1 Fluidized beds

Fluidization is a phenomenon which occurs when a bed of solid particles is subjected to a gas flow passing though the bed in an upward direction [7]. At low gas velocities, the gas merely percolates through the voids of the particles. This is referred to as a fixed bed. If the gas flow rate is increased, the particles will move apart and the bed will expand. However, if the gas has a sufficiently high velocity, the drag forces from the gas on the particles will be equal to the gravitational force on the particles and the bed will be suspended in the gas flow. When in this suspended state, the bed will behave in a fluidlike manner. The gas velocity at which the transition from the fixed bed state to the fluidized state occurs is referred to as the minimum fluidization velocity, u_{mf}. At higher gas flow velocities, above the minimum fluidization velocity, the excess gas will form bubbles or channels as it passes through the bed. The movement of the bed particles will also be increasingly vigorous. The bed is then in a state referred to as bubbling fluidization. At very high gas velocities, it is possible for bed particles to be carried out of the reactor along with the gas flow. The velocity at which this starts to occur is referred to as the terminal velocity, u_t.

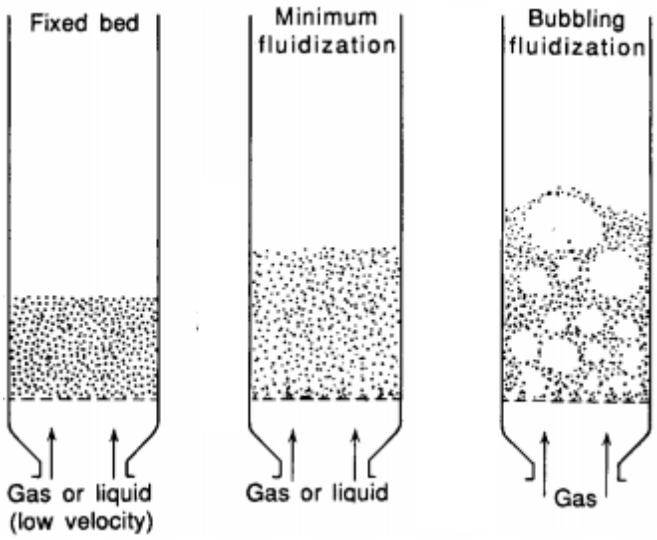

Figure 2: Different states of fluidization, depending on the gas velocity [7].

The high level of mixing of the bed particles, along with the very high surface area contact between the bed particles and the fluidizing gas per unit of bed volume, makes a high rate of mass transfer between the solid and fluid phases possible [9]. This makes fluidizing beds an option for processes where a chemical reaction between a solid phase and a fluid phase takes place, the solid phase being the bed particles and the fluid phase as a part of the fluidizing gas. Fluidized beds also have a high amount of particle-particle and particle-wall collisions, which combined with the mentioned advantages leads to a high heat transfer rate between the solids, fluid and any wall surface in contact with the bed.

When considering energy conversion processes, other advantages include higher combustion efficiency, lower operating temperatures and greater fuel flexibility than alternative technologies [10]. This makes them a good option for combustion of biomass, waste and, in some cases, coal. Other application areas include chemical processes, mineral processing, particle coating and drying.

2.2 Heat transfer in fluidized beds

The high heat transfer capacity of fluidized beds is often one of the main reasons for their usage. They are able to supply or remove large quantities of heat as a function of reactor size, depending on the demands of a process. The temperature of the bed is rather uniform, both in the axial and radial direction, as long as the gas flow sufficiently mixes the bed [7]. A key parameter is the heat transfer rate between the bed and a heat exchanging wall surface. At the wall, heat is transferred from hotter to colder surfaces through contact between bed particles, fluid and the wall area. These interactions include particle-particle, particle-fluid, particle-wall and gas-wall heat exchange. These contacts are temporary and are continuously made and destroyed by the movement of the bed [11]. At high temperatures, radiation from the bed particles contribute notably to the heat transfer rate.

Through these conductive, convective and radiative mechanics, heat will be transferred to the wall from the bed particles near the wall. As these bed particles closest to the wall are cooled down, they are replaced by new ones due to the movement of the bed and the temperature difference between the bed and wall is maintained.

Numerous studies and correlations for the bed-to-wall heat transfer coefficient have been made, in attempts to determine which process parameters are important [7,12]. The results are not universal, due to the complex nature of bed-to-wall heat transfer. A number of observations can be made for comparison with the experimental results for packed beds, generated in this thesis.

An increase in the void ratio of the bed leads to a decrease of the heat transfer coefficient, as the amount of bed particles available for transferring heat has decreased. An increase of the velocity of the fluidizing gas, at low gas velocities, results in an increase of the heat transfer coefficient. At higher velocities, the heat transfer coefficient reaches a maximum value, to then remain close to constant as the gas velocity increases further [13]. Lastly, an increase of the bed temperature leads to an increase of the heat transfer coefficient. Kunii & Levenspiel suggests this is partly due to the increased radiation heat transfer and partly to increased thermal conductivity of the fluidizing gas at higher temperatures [7].

Almost no data currently exist for high temperature heat transfer in fluidized beds containing packing, which is the subject of study in this thesis. So, the degree of novelty in this work is high.

2.3 Bubble formation and its effect on the solid-gas reaction rate

One of the core factors in fluidized bed reactors is the formation and growth of bubbles inside the bed. As gas enters at or near the bottom of the bed, small bubbles are formed. As the flow rises in the reactor, these small bubbles coalesce into bigger ones [7]. For large-scale reactors, with deep beds, the bubbles can grow to a very large size. In some scenarios, depending on the diameter and height of the bed, it is possible for gas bubbles to grow to a size so large that they spread across the entire width of the reactor vessel. The result is a flow pattern known as slugging. The diameter of the bed particles heavily influences the maximum diameter of the bubbles, by limiting the maximum size they can grow to before splitting. Coarser particles allowing for a greater maximum size, and very large particles allowing for seemingly limitless growth [7].

As previously mentioned, fluidized beds provide a very large contact area between the solid phase and the fluid phase, making it ideal for fluid-solid chemical reactions. The mass transfer between the gas and fluid phases could be assumed to take place at the boundary between the phases, i.e. the surface of the gas bubbles [9]. However, as gas bubbles coalesce inside the bed, the total amount of contact area between the phases decreases, as the ratio between a bubble's surface area and

volume decreases with increasing bubble diameter. As the total surface area available for mass transfer decreases with bubble growth, so does the corresponding reaction rate inside the bed [14]. Thus, to achieve higher reaction rates, the reduction of the diameter of the fluid bubbles is of high interest.

2.4 Bubble growth inhibition by introducing packing materials

It is possible to limit the size of the gas bubbles by physically restrict their growth inside the bed. Traditionally this would be done by introducing a fixed device into the bed, such as metal bars or a grate. However, the fixed nature of these applications makes them difficult to maintain. A solution could be the use of a packing material [8], which could easily be removed from the reactor between operations, as it is not attached. An individual piece of packing would be much larger in size than a bed particle. When a large number of these packing materials are introduced to the reactor, they would stack at the bottom of the bed with the bed particles occupying the voids between the packing material. As the bed is subjected to a sufficiently large gas flow, bed particle fluidization and gas-solid reaction would take place in these voids as well.

The main purpose of the packing material would be to physically restrict bubble growth. However, by introducing it to the reactor, most operating conditions are altered. The mixing inside the bed is hindered, as the movement paths of the bed particles are restricted. The packings would also physically cover part of any heat exchange surfaces in the reactor, reducing the area available for heat transfer into or out of the bed. Concerning the material properties of the packings, the material must be able to withstand the chemical operating conditions and the bed temperature of the reactor.

Packings are commonly found in the chemistry industry, in processes involving gas absorption, distillation and phase separation [15]. They are a design alternative to the tray design found in distillation column. There are two separate categories of packings, random and structured packings. The structured packings are placed in a specific pattern inside the column, while random packings are inserted in a more non-specific configuration. The packings used in this thesis, Raschig, Hiflow® and RSMR, are classical examples of random packings used for distillation purposes. They are designed to have a large amount of surface area per unit volume, to maximize the available area for vapour-liquid equilibria, and a high amount of void space per unit volume, while minimizing friction with the fluid flows through open shape designs with good aerodynamics. The high void factor and low friction, open shape designs are attractive properties when considering packings for use in fluidized beds.

2.5 Pressure drop across fluidized beds

Fluidizing a particle bed with a gas flow results in a pressure drop across the bed. At full fluidization, the pressure drop is equal to the effective weight of the bed, see eq. (3) [7].

$$\Delta P_{bed} = H(1 - \varepsilon_{bed})(\rho_s - \rho_g) \tag{3}$$

Further increasing the gas velocity after full fluidization is reached will not significantly increase the pressure drop, as the bed will expand to facilitate the increasing gas flow. Worth noting is that as the pressure drop per unit of bed height is a constant property of the fluidized bed.

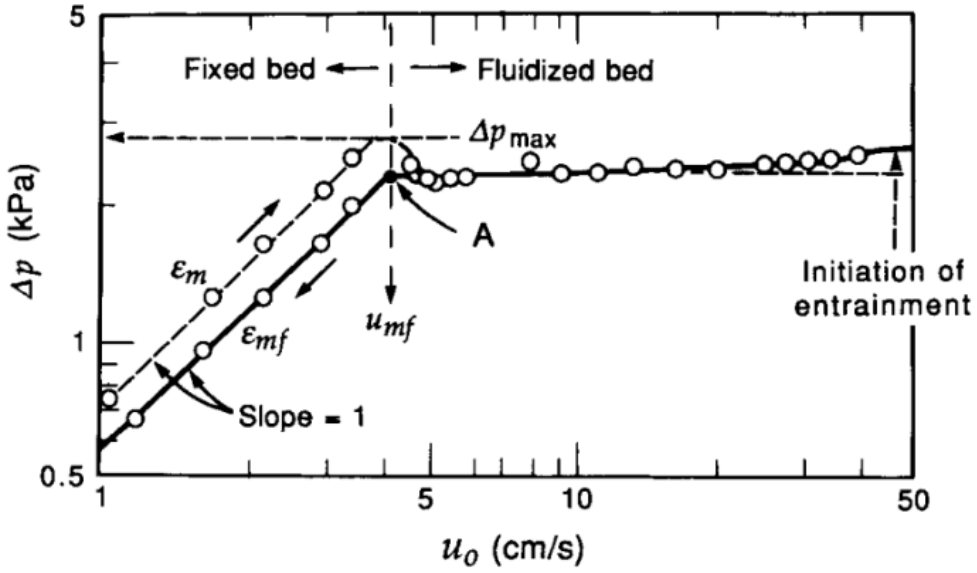

Figure 3: Textbook example of the behavior of the bed pressure drop for varying superficial gas velocities [7].

If packing material is introduced to the bed, it affects the pressure drop. Sutherland et al. experienced a decrease in bed pressure drop per unit height [16], which could be attributed to the lower mass amount of bed particles present in the bed as the packing occupies part of the volume. However, if the pressure drop per mass amount of bed material is considered, then the pressure drop is higher for packed beds, as evaluated by Donsí and Ferrari, as well as Aronsson et al. [8,17]. The reason could be that due to the packing, the particle bed is not able to deform as easily to accommodate the passing gas flow, resulting in a higher bed pressure drop.

2.6 Vertical segregation of packing and fluidized bed particles

A bed which contains a stationary packing material and a fluidizing bed particle material will have two distinct regions when fluidized by a gas flow. A bottom region made up of the packing material and the voids between them, and a region on top of the packing [17]. As the bed is fluidized, the velocity of the gas flow will be different in the two regions. In the packing region, the average cross-section area the flow passes through will be lower, due to the packing material. The gas velocity will therefore be higher. As the gas exits the packing region and enters the top region, the gas velocity decreases. The high gas velocity inside the packing, combined with that the bed expands in general when fluidized, results in that a portion of the fluidizing bed particles are pushed into the top region, forming a segregated top layer, see figure 4. This top layer is assumed to have the same properties as a fluidized bed containing no packing material, but operating under the same conditions as in the packed case.

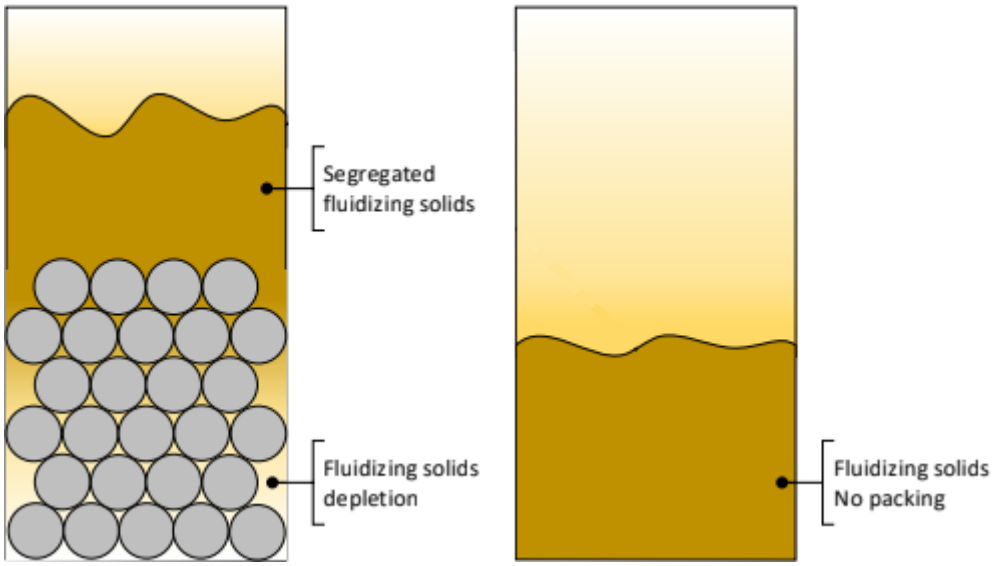

Figure 4: Picture showing the resulting vertical segregation when packing is added to a fluidized bed [8].

3 Method

3.1 Experimental Setup

The experimental work was conducted in a cylindrical laboratory-scale bubbling fluidized bed reactor made from 253 MA steel, with an inner diameter of 77.92 mm. Air was used as the fluidization gas, which was fed into the reactor by mass flow controllers. The gas entered the reactor first through a windbox, then through a distribution plate into the bed. The distribution plate was 5 mm thick and contained 61 0.6 mm holes. No fuel was used, and the heat for the experiments was supplied by an electrical furnace which enclosed the reactor. As the windbox was located inside the furnace, the fluidization gas was pre-heated to temperatures close to the bed temperatures before entering the bed. The heated gas exiting the reactor was collected by a ventilated hood.

The reactor contained a single horizontal tube running through it, made of Inconel alloy 600. The tube had an inner diameter of 4 mm and outer diameter of 6 mm. It was positioned 75 mm above the distribution plate. Water flowed through the tube, sourced from a tap. Its flow rate was regulated by a valve. The water was collected and weighed by a scale after exiting the reactor, to precisely determine its flow rate. The temperatures of the flow at the inlet and outlet were measured by thermocouples. It should be noted that the tube part past the outlet had to be bent to circumvent an inclined pipe. The outlet thermocouple could therefore not reach the outlet position inside the horizontal tube and only measured the outlet temperature at a position approximately two centimetres away from the outlet. A previous experiment, done for the same reactor and a similar experiment, concluded that the difference from the real outlet temperature was negligible [13].

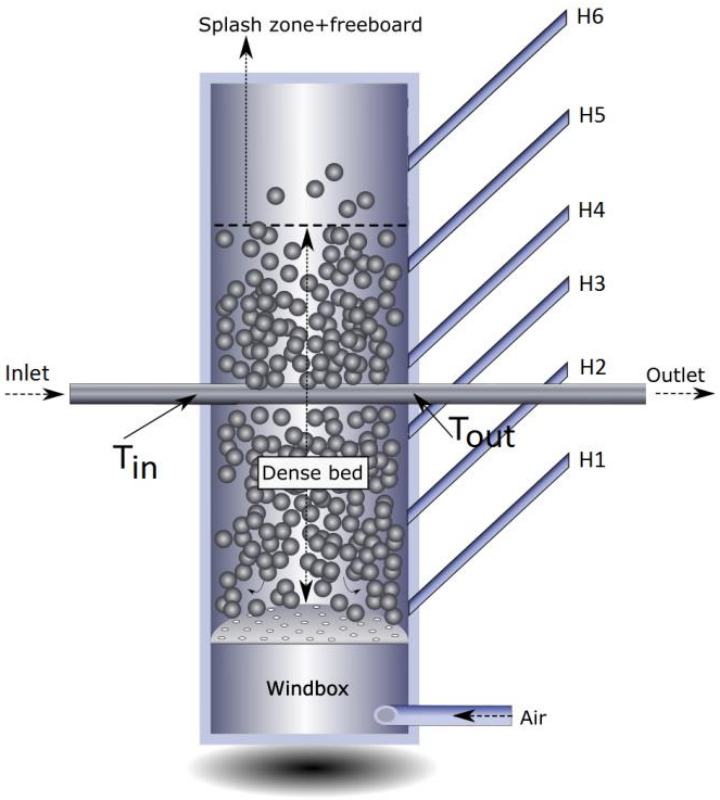

Figure 5: Illustration of fluidized bed reactor setup [12].

A number of pipes, inclined at 45°, were connected to bed through the side wall of the reactor, to allow for pressure and temperature measurements at the positions where they entered the bed. See table 1 for the position of the measurement points. Pressure was measured with pressure transducers in positions 2, 5, 7 and 8, as well as in the tube supplying the fluidization gas. Temperature was measured with thermocouples in positions 1, 3, 4, 6, as well as in the windbox. The thermocouples in positions 1, 3, 4, 6 were inserted 10 mm into the bed, at the inclined angle of 45°. When gathering data, the pressure and temperature values were recorded once per second for a 60 second period. For each measurement, the average water flow rate was determined by gathering 60 seconds worth of flow, weighing it with a scale and dividing it with the density of water based on the average water temperature in the tube. The calculations required that a temperature measurement was designated as the temperature of the bed. The temperature in position 1 was chosen on the basis that it would be the least affected by the cooling effect of the water flowing through the horizontal tube, as it was the measurement point furthest from the tube.

Table 1: Height of measurement positions, in relation to the distribution plate.

Position	Height [mm]
1	30
2	47
3	65
Water tube	75
4	105
5	130
6	150
7	310
8	605

The fluidizing bed material used in all experimental configurations was B-28 silica sand sourced from Baskarp, supplied by Sibelco Nordic AB. It was sieved to particle sizes within the interval 212-300 µm. Using sieves for particle sizes 212, 250, 300 and 355 µm, the weighted mean particle diameter for the used interval was estimated to be 250.2 µm. The bulk density was determined by pouring a mass of the bed material into a known volume, giving a bulk density value of 1594 kg/m^3.

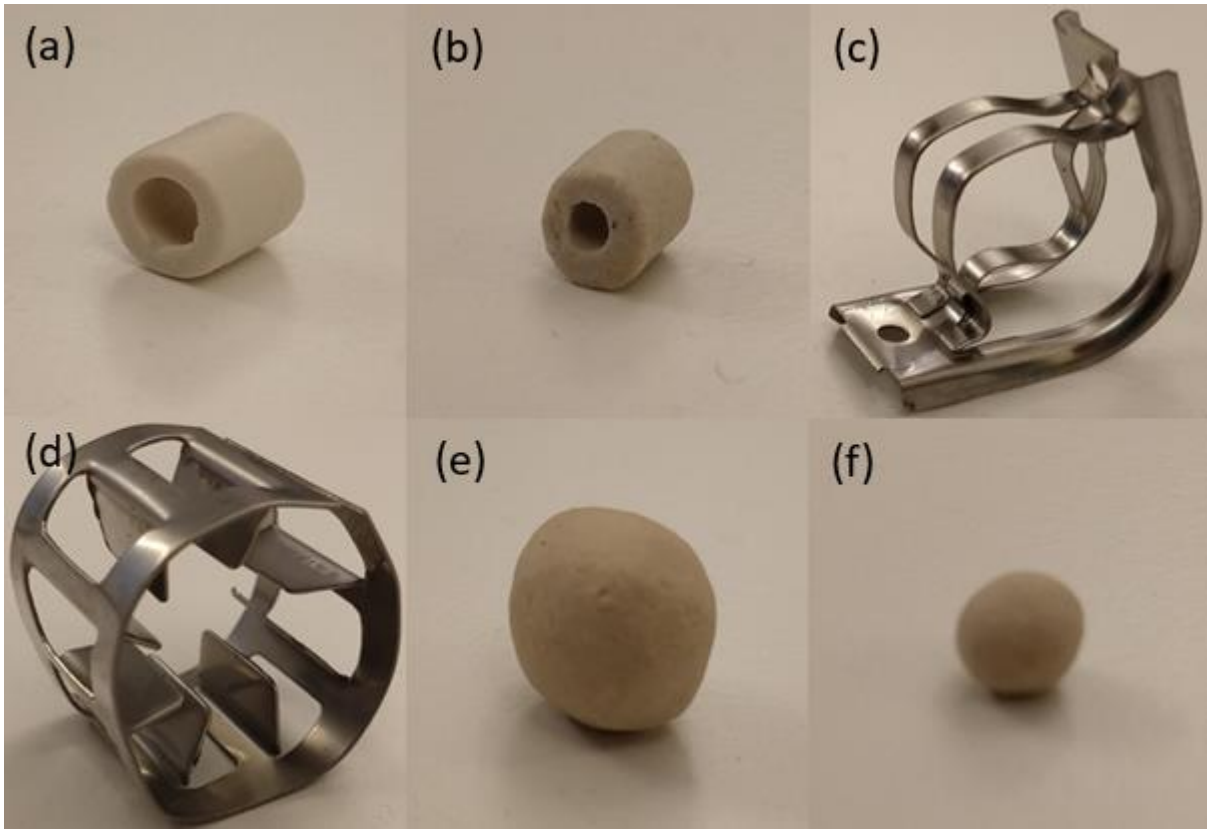

Figure 6: Packings that were experimentally evaluated. (a) 10 mm Raschig ring, (b) 6 mm Raschig ring, (c) RMSR saddle ring, (d) Hiflow® ring, (e) ½" Aluminium silicate ball, (f) ¼" Aluminium silicate ball

Six different packings were initially considered. Two types of spherical packings, both made of aluminium silicate. A larger one with a diameter of half an inch and a smaller one with a diameter of a quarter of an inch. Two packings were differently sized ceramic Raschig rings, with a diameter of 6 mm and 10 mm respectively. Two packings were supplied by RVT Process Equipment GmbH, a 25 mm stainless steel RMSR 25-3 packing and a 25 mm stainless steel Hiflow® ring 25-5 metal packing. All packings were of a sufficient size and density to not display any fluidizing behaviour during the experiments, but instead stack at the bottom of the reactor. The amount of packing and fluidizing bed material was chosen as to fill the reactor to a height of 13 cm at rest, with the fluidizing bed material filling up the packing voids. The required packing and fluidizing bed material mass was estimated by filling a container of a similarly sized and shaped volume as the corresponding reactor bed volume. With the container placed on a scale, the packing was first added to a height of 13 cm and its mass recorded. The packing voids were then filled with silica sand up to the same height, with the mass of added sand recorded. The void fraction of the packings was estimated by pouring a packing into a container with a known volume, placing the container on a scale, filling the voids in the packing with water, recording the change in mass and dividing it by the density of water to calculate the volume of the voidage.

Table 2: Description of the experimental cases, with a bed containing no packing as a reference case. All beds had a height of 13 cm when at rest.

Packing	Void fraction of packing [-]	Mass of packing material [g]	Mass of silica sand [g]
¼" Aluminium silicate balls	0.34	897.9	340.3
½" Aluminium silicate balls	0.38	872.7	438.2
6 mm Raschig rings	0.45	686.1	559.0
10 mm Raschig rings	0.52	586.7	619.1
RMSR 25-3	0.85	133.6	967.8
Hiflow® ring 25-5 metal	0.84	162.3	931.8
Bed with no packing	-	0	988.1

The controllable parameters during the experiments were the water flow rate, the superficial gas velocity and the bed temperature. The water flow rate was kept constant at 20 ml/s, a flow rate which previously had been verified to be high enough to prevent boiling in the tube and give turbulent flow conditions [12]. The bed temperature was varied between 400°C and 900°C. The superficial gas velocity was varied between 0.04 m/s and 0.411 m/s. When the bed temperature or superficial gas velocity was being varied, the other was kept at a base case value, see table 3.

Table 3: Values for the base case of the parameters.

Parameter	Base case
Water flow rate	20 ml/s
Bed temperature	800°C
Superficial gas velocity	0.20 m/s

3.2 Calculations for obtaining the bed-to-tube heat transfer coefficient

The measured values of the inlet and outlet water temperatures, the water flow rate and the bed temperature formed the basis for calculating the bed-to-tube heat transfer coefficient.

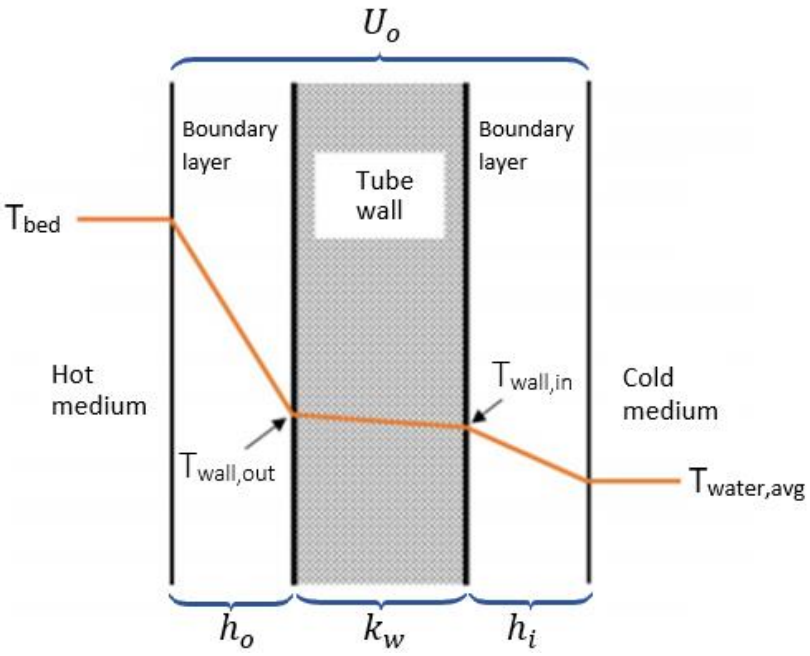

Figure 7: Thermal resistances for the heat transfer from the fluidized bed to the water flow [12].

The amount of heat transferred from the bed to the water flow, Q, was estimated using the water flow rate and the difference of the outlet and inlet water temperature, see eq. (4). The values of the water density and heat capacity were taken at the average of the inlet and outlet water temperatures, and the resulting calculated values are the average values over the length of the tube.

$$Q = \rho_{water}\dot{V}c_{Pwater}(T_{water,out} - T_{water,in}) \quad (4)$$

The bed-to-tube heat transfer coefficient, h_o, was calculated by using an equation for the overall heat transfer coefficient for heat transfer through a tube, see eq. (5) [18].

$$U_o = \frac{1}{\frac{d_o}{d_i h_i} + \frac{d_o \ln(d_o/d_i)}{2k_{wall}} + \frac{1}{h_o}} \quad (5)$$

The values of the overall heat transfer coefficient, U_o, the tube-to-water heat transfer coefficient, h_i, and the thermal conductivity of the tube, k_{wall}, must be determined before h_o can be calculated. By using the equation for heat transfer between two flows, U_o can be determined, see eq. (6).

$$Q = U_o A_o \Delta T_{LM} \tag{6}$$

$$\Delta T_{LM} = \frac{\Delta T_{in} - \Delta T_{out}}{\ln\left(\Delta T_{in}/\Delta T_{out}\right)}$$

$$\Delta T_{in} = T_{bed} - T_{water,in}$$

$$\Delta T_{out} = T_{bed} - T_{water,out}$$

T_{bed} is the temperature of the packed fluidized bed, which is assumed to be constant along the horizontal direction of the tube when calculating the temperature differences used in the logarithmic mean temperature difference, ΔT_{LM}. $T_{water,in}$ and $T_{water,out}$ are the tube inlet and outlet water temperatures.

The heat transfer coefficient between the inside wall of the tube and water flow was estimated using the average of three correlations, see eq. (7)-(9) [19]. The correlations can be considered to be valid for liquid phase and turbulent flows. A Reynolds number of 6345 was calculated based on the chosen water flow rate of 20 ml/s, satisfying the turbulence criterion [18]. The highest value of the outlet water temperature that was measured during the experiments was 31.2°C, far below the boiling temperature of water, which satisfied the single-phase criterion.

$$h_i = 0.023 \frac{k_{water}}{d_i} Re^{0.8} Pr^{0.4} \tag{7}$$

$$h_i = \frac{k_{water}}{d_i} j_h RePr^{0.33} \tag{8}$$

$$h_i = \frac{4200(1.35 + 0.02T_{water,avg}) u_{water}^{0.8}}{d_i^{0.2}} \tag{9}$$

k_{water} is the heat transfer capacity of water, u_{water} the average velocity of the water flowing through the horizontal tube, Pr is the Prandtl number and j_H is the heat transfer factor for the inside of the horizontal tube.

The value of the thermal conductivity of the tube wall was estimated at the average temperature of the tube wall [20]. The temperature of the inner side of the tube, $T_{wall,in}$, was estimated using the tube-to-water heat transfer coefficient, see eq. (10).

$$Q = h_i A_i \left(T_{wall,in} - T_{water,avg}\right) \tag{10}$$

An equation for the heat transferred through the tube wall was used to determine the temperature on the outer side of the tube, $T_{wall,out}$, but the thermal conductivity used in the equation is in turn dependent on the outer tube wall temperature. A solution was found iteratively by initially guessing the outer wall temperature $T_{wall,out}$, see eq. (11)-(13).

$$T_{wall,avg} = \frac{T_{wall,out} + T_{wall,in}}{2} \tag{11}$$

$$k_{wall} = f(T_{wall,avg}) \tag{12}$$

$$Q = \frac{2k_{wall}}{d_o \ln(d_o/d_i)} A_o (T_{wall,out} - T_{wall,in}) \tag{13}$$

The bed-to-tube heat transfer coefficient can now be determined using equation (5).

3.3 Calculations for vertical separation of fluidizing particles and packing

As a packed bed is fluidized, a portion of the fluidized bed particles segregate from the packing material and form a layer in a region on top of the packing. If this region is assumed to have the same properties as a bed containing no packing, then the mass of the bed particles occupying the volume above the packings and the volume between the packings can be estimated. By placing a pressure sensor at the height in the reactor where the packed region ends, the pressure drop over the fluidized bed region above the packing can be measured. This region will have the same mass of bed material per pressure drop ratio, $m_{bp}/\Delta P$, as a bed containing no packings but with the same superficial gas velocity. These ratios were measured separately by measuring the pressure drop over a bed containing a known mass of fluidizing bed particles, for the relevant superficial gas velocities. By multiplying the pressure drop over the region above the packing of a fluidized packed bed with the mass per pressure drop ratio, the mass of fluidized bed particles in that region can be estimated, see eq. (14).

$$m_{bp,top} = \Delta P_{top} \left(\frac{m_{bp,top}}{\Delta P_{top}} \right)_{No\ packing} \tag{14}$$

The fluidizing bed particles inserted into the reactor were weighed beforehand, making a mass balance possible. The mass of fluidizing bed particles in the volume between the packings can be estimated using eq. (15), with the assumption being that no bed particles are lost by exiting the reactor with the gas flow.

$$m_{bp,tot} = m_{bp,pack} + m_{bp,top} \tag{15}$$

The void fraction of the volume between the packings is related to the mass of the bed particles within that volume. The relation between the void fraction and fluidizing particle mass for the intra-packing volume is given by eq. (16). The void fraction for a stationary bed is the void fraction of the bed particles at rest.

$$\varepsilon_{bp,packing} = \left(\frac{1-\varepsilon_{bp}}{m_{bp,tot}}\right) m_{bp,top} + \varepsilon_{bp} \tag{16}$$

3.4 Pressure drop across packed fluidized beds

Two different ways of evaluating the pressure drop across a packed bed were used. The first was the pressure drop per unit of bed height, to evaluate how the pressure drop changes with bed height. The second way was the pressure drop per unit of bed mass, to evaluate how the pressure drop was affected by packing material-bed particle interactions.

The pressure drop over the packing material region is measured by a pressure sensor placed at the height where the region ends, which for all cases was 13 cm above the distribution plate. The pressure drop per unit of bed height for the different packing material cases was thus estimated.

As mentioned in the theory section, the pressure drop across a fluidized bed containing fluidizing bed particles but no packing, is mainly dependent on the mass of the bed material. A ratio between the pressure drop over a fluidized bed and the mass of the bed, $\Delta P/m_{bp}$, can thus be estimated by measuring the pressure drop over a known weight of fluidized bed mass. In packed beds, the pressure drop also depends on the type of packing material [8]. As the pressure drop over a bed containing packing material, but no fluidizing bed material is close to zero, any deviation from the pressure drop per mass ratio from the case with no packing can be attributed to some sort of packing-bed particle interaction. The mass balance from the vertical separation calculation section provided the mass of bed particles present in the volume between the packings. The pressure drop per mass of fluidizing bed material over the packing region could thus be estimated.

4 Results

The results are divided into two sub-section, with the first section evaluating the effect of varying the bed temperature and the second section the effect of varying the superficial gas velocity. Numerical data corresponding to the values presented in the graphs is available in appendix B. Graphs containing the total pressure drop over the beds, along with the pressure drop over the region containing packing and the fluidized bed region on top of the packing, are available in appendix A. The data from the ¼" aluminium silicate balls case is excluded from the report, as no measurements taken during the experiment indicated that the packed bed was properly fluidized. The pressure sensor positioned at the end of the packed region of the bed registered no rise in pressure when the bed was subjected to the maximum superficial gas velocity, which indicated that the bed had not expanded due to fluidization and risen above the sensor. Additionally, the resulting bed-to-tube heat transfer coefficient values that were calculated were close to half that of those of the worst performing case, the 6 mm Raschig rings. In prior experiments using the ¼" ASB, in an acrylic reactor, the bed particles were observed to gather along one side of the bed, with significant amounts of the fluidizing gas bypassing the bed particles [8].

4.1 Bed temperature variation

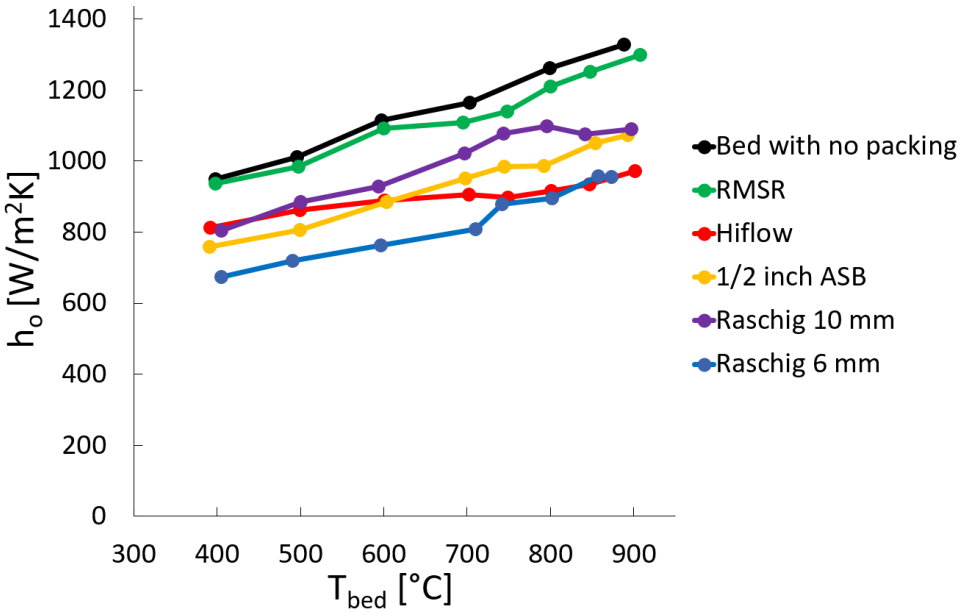

Figure 8: Experimentally estimated heat transfer coefficient at different bed temperatures.

The resulting heat transfer coefficients from varying the bed temperature can be seen in figure 8. For some cases, the bed temperature was unable to reach the highest desired measurement point of 900°C, due to reaching the maximum capacity of the furnace. The heat transfer coefficient increased with increasing bed temperature for all packings, but all performed worse than a bed containing no packing material at all. Worthy of note is that the Hiflow packing performed significantly worse than the RMSR packing, despite many similar attributes except for shape. It also had a less significant increase in heat transfer coefficient with increasing bed temperature than the other packings. Concerning the RSMR packing, it performed almost equally well as the bed with no packing.

4.2 Superficial gas velocity variation

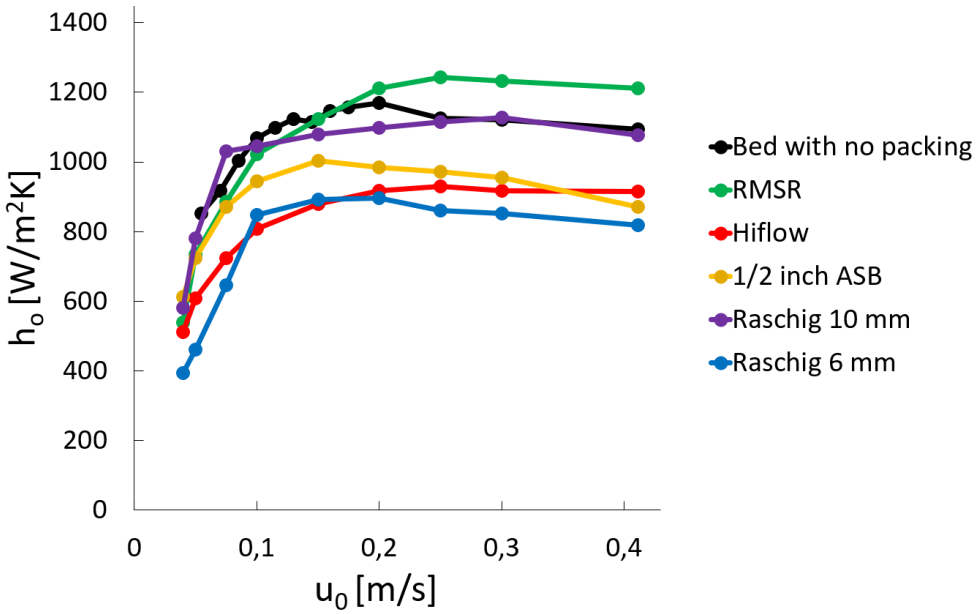

Figure 9: Experimentally estimated heat transfer coefficient at different superficial gas velocities.

The resulting heat transfer coefficients of varying superficial gas velocities can be seen in figure 9. In all cases, the heat transfer coefficient increased sharply at lower velocities, before levelling out and reach a maximum heat transfer coefficient value. After the maximum value, h_o decreased slightly with increasing superficial gas velocity. Once again, the Hiflow packing performed poorly compared to the RMSR packing, which even outperformed the bed containing no packing at high velocities.

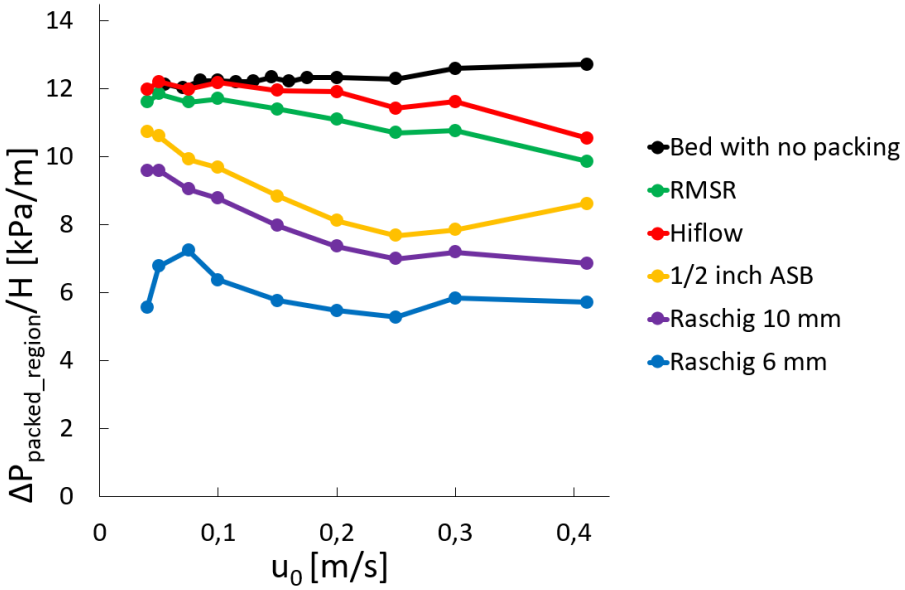

Figure 10: Packed bed pressure drop, ΔP_{packed_region}, per unit of bed height, at different superficial gas velocities. The pressure drop is measured over the region of the bed which contains packing material, described in section 2.6. The estimated values are scaled with the height of the packed region of the bed, 13 cm.

The pressure drop per unit of height of varying superficial gas velocities can be seen in figure 10. The pressure drop was measured over the 13 cm tall region of the bed which contained packing material. In all packing cases but for the ½" ASB, a general trend of decreasing pressure drop with increasing superficial gas velocity can be seen. The pressure drop of the ½" ASB packing also has a decreasing trend at lower velocities, but increases at higher velocities. Worth noting is that all beds with packing have smaller pressure drops per height than the bed which contains no packing.

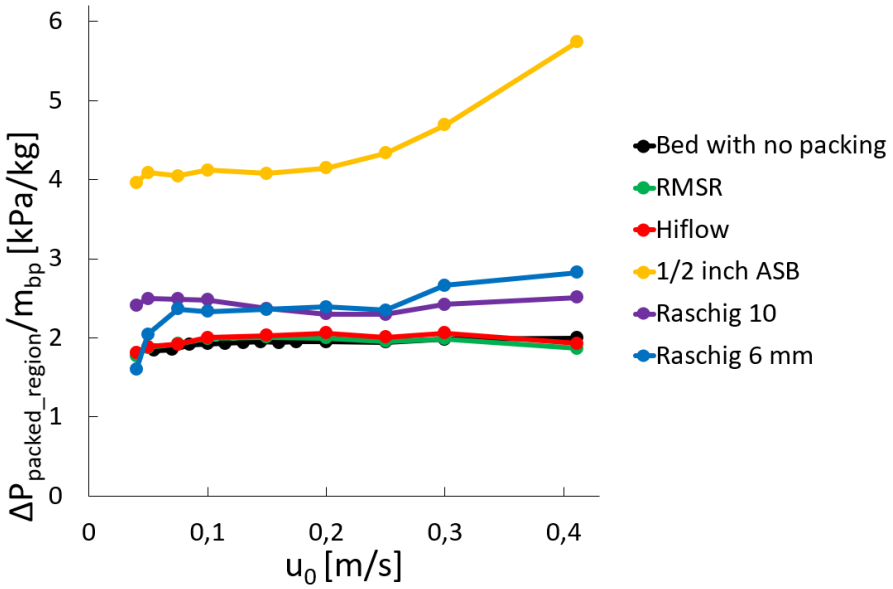

Figure 11: Packed bed pressure drop, ΔP_{packed_region}, per mass amount of fluidizing bed material, m_{bp}, at different superficial gas velocities. The pressure drop and fluidizing bed material mass are estimated over the region of the bed which contains packing material, described in section 2.6.

The pressure drop per mass amount of fluidizing bed material of varying superficial gas velocities can be seen in figure 11. The pressure drop and mass amount are estimated for the 13 cm tall packed region. The pressure drop per mass amount is constant for the RMSR and Hiflow packings, but the lower void ratio packings, the Raschig rings and especially the ½" ASB packing, display increasing pressure drop per mass amount at higher velocities. Overall, the ½" ASB packing also has a significantly higher pressure drop per mass amount than the other packings.

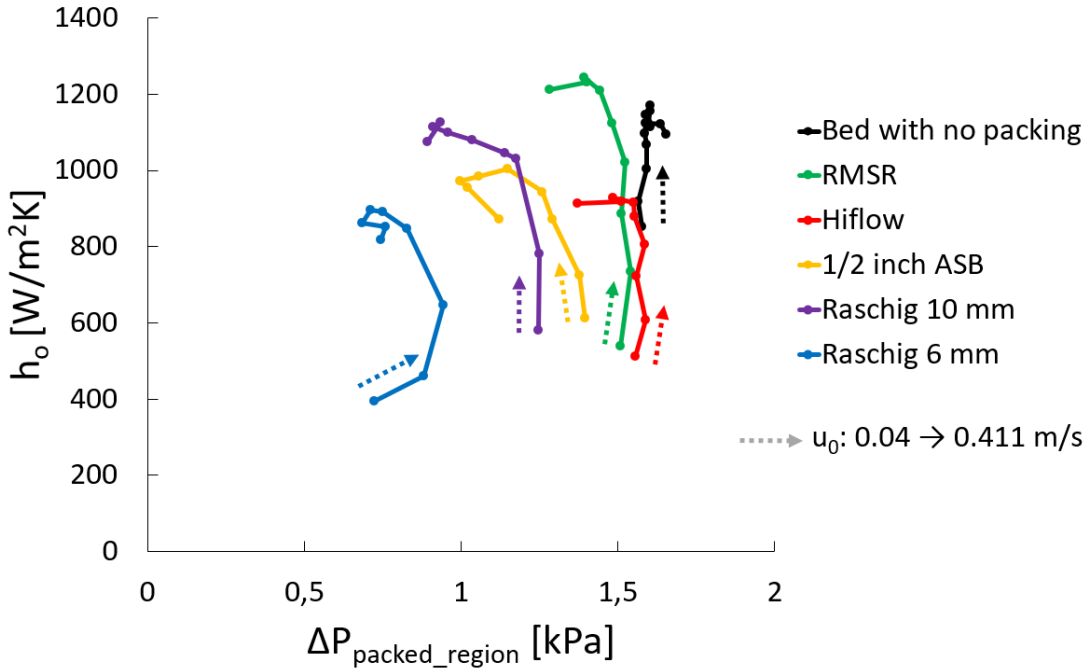

Figure 12: Packed bed heat transfer coefficient and the corresponding packed region bed pressure drop, at different superficial gas velocities.

The heat transfer coefficient and the corresponding packed region bed pressure drop, for varying superficial gas velocities, can be seen in figure 12. The arrows indicate the direction for the increasing gas velocity. As can also be seen in figure 9, at lower gas velocities the heat transfer coefficient increases with increasing gas velocity for all packings. The heat transfer coefficient then reaches a maximum and slowly decreases with further increasing gas velocity. At lower gas velocities, the pressure drop of the packings, as also seen in figure 10, all decreased with increasing gas velocity. The pressure drop of the low void ratio packings, the Raschig rings and the ½" ASB, decreased more sharply than for the RMSR and Hiflow packings. At high velocities, the pressure drop continues to decrease for the RMSR and Hiflow packings, while the Raschig rings pressure drop stabilizes and the ½" ASB pressure drop increases.

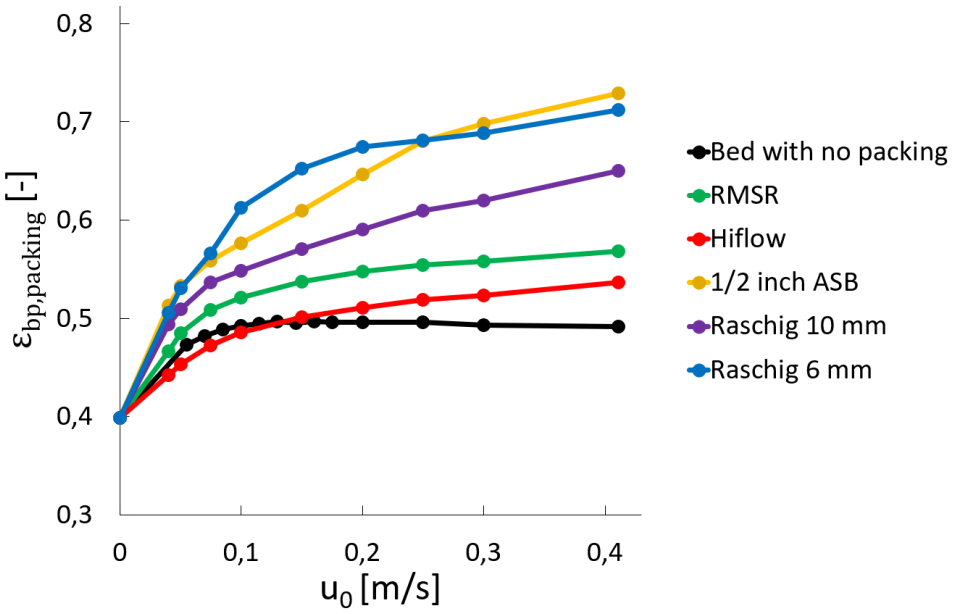

Figure 13: Void fraction of the volume between the packing materials at different superficial gas velocities.

The void fraction of the volume between the packing material of varying superficial gas velocities can be seen in figure 13. The starting value of all cases is the void fraction value of the bed material at rest. Two distinct intervals with regard to the superficial gas velocity can be observed. At lower velocities, the void fraction increases rather sharply, while at higher velocities it increases at a slower rate. For the bed containing no packing, the void fraction does not change at all at higher velocities.

5 Discussion

The discussion section features sections containing the experimental results, possible error sources and possible areas for further research.

5.1 Experimental results

5.1.1 Heat transfer coefficient

The main purpose of the project was to evaluate the performance of the six packing materials, in how the bed-to-tube heat transfer coefficient and bed pressure drop were affected by varying the bed temperature or the superficial gas velocity in a packed fluidized bed. When considering the results, it should be kept in mind that the project does not study the main benefit of using packing materials, which is the prevention of the growth of gaseous fuel bubbles, but rather the expected drawbacks in decreased heat transfer and increased bed pressure drop.

In all cases the bed-to-tube heat transfer coefficient increased in a linear trend with increasing bed temperature. All cases also had the same trend of sharply increasing heat transfer coefficients at low superficial gas velocities, followed by a maximum and slow decrease at higher velocities. Both behaviours are present in beds containing no packing [7,13]. When evaluating each individual packing type, three major effects should be considered. The packing material will cover part of the outer surface of the horizontal tube, which decreases the available area for bed particle-tube surface heat transfer. The packings will hinder the movement of bed particles by, at certain points in the bed, constricting the path the particles can move through. Work done by Sutherland et al., using spherical packings, found that particle movement was more restricted with smaller packing diameters [16]. The amount of fluidizing bed material present in the volume between the packing material decreases with increasing superficial gas velocity, as is seen in figure 13. This could be expected to negatively affect the heat transfer coefficient, as there are fewer bed particles present to transfer heat by fluidizing.

The packing with the highest heat transfer coefficient values was the RSMR packing. Its saddle shape provides large openings to prevent constriction, independent on which general direction an incoming bed particle moves in. The shape also considerably limits the horizontal tube surface area which can be covered, regardless of how it is positioned against the tube. The low void fraction results in only moderate vertical segregation. It outperformed the bed with no packing at high superficial gas velocities. The reason is likely because the gas bubbles grow large in size, due to the high gas flow at these velocities, and are able to cover the heat exchange surface of the horizontal tube to a large degree. As the heat transfer capacity of the gas phase is lower than that of the bed particles, the heat transfer rate will decrease. If the RMSR packings are introduced to the fluidized bed, the bubbles will be split into smaller size, allowing for more bed particles to come into contact with the heat exchange surface and the heat transfer capacity to increase.

The Hiflow packing performed worse than the RSMR, even though both have the same void fraction value. The larger surface areas on the outside of the ring are able to cover more of the horizontal tube surface. The large fins in the centre could also possibly restrict the movement of the fluidized bed particles. Regarding vertical bed separation, it has the lowest values of all packings, even retaining more bed particles at lower superficial gas velocities than the bed which contained no packing.

The 10 mm Raschig ring packing had higher heat transfer coefficient values than the 6 mm Raschig ring, for all evaluated reactor operating conditions. The difference was especially large at high superficial gas velocities. The reason could be due to the size difference of the packings resulting in

differently sized constricting points in the packed region of the bed. As Sutherland et al. experienced, the smaller packing diameters would hinder the movement of the bed particles more. This effect becomes even more pronounced for Raschig ring shaped packings, as the channel in the middle of the packing could be considered such a constricting point. The higher vertical segregation of the 6 mm Raschig ring results in a lower heat transfer coefficient, further increasing the difference with the 10 mm packing.

The ½" ASB packing performs slightly worse than the 10 mm Raschig ring when considering the heat transfer coefficient for varying bed temperatures, even though its larger diameter should give it an advantage due to less bed particle movement constriction. The difference in the heat transfer coefficient values increases with increasing superficial gas velocity. The reason could be due the higher degree of vertical segregation experienced by the ½" ASB at high velocities, due to its lower void fraction in the packing. Overall, the spherical shape performed worse than the cylindrical shape, from a heat transfer perspective.

5.1.2 Pressure drop over the packed region of the bed

In general, the pressure drop over a set bed height decreases when packing is inserted into it [8,16]. As packing is introduced, the volume the fluidizing bed particles can occupy is restricted to the volume between the packings, which depends on the void fraction of the packing material. When the amount of fluidizing bed material decreases, so does the total amount of downward pressure it exerts. The pressure drop per height also decreases with increasing superficial gas velocity. The reason is likely due to the decreasing amount of bed material present in the packed region with increasing velocities, due to the increase in vertical segregation between the bed particles and the packing, seen in figure 13.

As a packed bed is fluidized, interactions between bed particles and packing material lead to an increase of the bed pressure drop. The reason could be due to the restriction of the available volume for the gas and particles to move through, when the packing material is introduced. The introduction of packings leads to a higher gas velocity in the packing voids. The higher gas velocities and constricted pathways through the packings will lead to an increase in the pressure drop over the packed region of the bed due to increased friction between the packings and the bed particles.

The RSMR and Hiflow had the highest bed pressure drops in absolute terms among the packings, but experienced the same pressure drop per mass amount of bed material as a bed with no packing. As such, little to no additional pressure drop due to bed particle-packing material interaction could be observed. This could be expected, as both packings have high void fractions, contain large opening and do not significantly constrict the movement of bed particles. Both experienced lower bed pressure drop with increasing superficial gas velocity.

The 10 mm Raschig ring had the second lowest absolute bed pressure drop, while the 6 mm Raschig ring had the lowest. They both had decreasing bed pressure drop with increasing superficial gas velocity. Both experienced higher bed pressure drop per mass amount of bed particles at all evaluated superficial gas velocities, especially in the 6 mm case at high velocities. This indicates that both packings cause some bed particle-packing material interaction. The Raschig rings will, at certain points in the packed region, constrict bed particle movement. The pressure drop over these points could cause the total pressure drop over the bed to increase. It is worth noting that in the 6 mm case, the pressure drop at superficial gas velocities below 0.1 m/s has the same behaviour as seen in not fully fluidized beds [7], seen in figure 3. The reason could be due to the packing restricting the movement of the bed particles, not allowing the particle bed to properly deform to accommodate the gas flow, as occurs at fully fluidized conditions. However, once the gas velocity reaches values

above 0.1 m/s, more than a third of the bed particles have moved into the top region due to vertical segregation, see figure 13. The increased voidage in the intra-packing volume provides the necessary conditions for the bed to accommodate the gas flow and fully fluidize.

The ½" ASB bed pressure drop decreased with increasing superficial gas velocity at low velocities but increased at high velocities for the evaluated range of gas velocities. This trend in the pressure drop differed from the other packings, but Aronsson et al. found similar behaviour in their work using the same ½" ASB packing material [8]. The high values of the pressure drop per mass of bed material indicate that the packing causes a significant amount of bed particle-packing interaction, especially at higher velocities where it rises sharply. The spherical shape of the packing material will cause particle movement constriction at certain points in the packing, increasing the total bed pressure drop.

5.1.3 Heat transfer coefficient and the corresponding pressure drop

The bed-to-tube heat transfer coefficient can be viewed as a beneficial parameter. The higher its value, the better the heat transfer ability of the bed over heat exchange surfaces. However, the bed pressure drop is not. A higher bed pressure drop will result in higher operating costs for the reactor. Figure 12, which combines the data from figures 9 and 10, shows the relation between heat transfer coefficient, bed pressure drop and superficial gas velocity for all packed beds and the bed without packing. As previously noted, the heat transfer coefficient increases with increasing gas velocity, for low gas velocities, while the bed pressure drop decreases for all packings. At higher velocities, the heat transfer coefficients reach a maximum value and then slowly decrease. The bed pressure drops of the RMSR and Hiflow packings continues to decrease, while the Raschig rings experience only slight changes in bed pressure drop and bed pressure drop of the ½" ASB increases.

By looking at figure 12, optimal superficial gas velocities can be suggested for each of the packings. The high void ratio RMSR and Hiflow show decreasing bed pressure drop without decreases in heat transfer coefficient at the highest gas velocities. The Raschig rings and the ½" ASB also show gas velocities where further increases in gas velocity would result in either no additional benefits or actively decrease the heat transfer coefficient while increasing bed pressure drop.

By looking at figures 9 and 10, or figure 12, a general trend can be seen where the introduction of packing material leads to a decrease in both the bed-to-tube heat transfer coefficient and the pressure drop of the bed. Apart from the RMSR at high velocities, the bed without packing has the highest bed-to-tube heat transfer coefficient. The reason is due to the packing material restricting the movement of the bed particles and covering heat exchange surfaces. The introduction of packings also leads to a lower mass amount of bed particles per unit of bed height, due to the packings occupying part of the bed volume. As seen in section 2.5, a decrease in bed particle mass leads to a decrease in the bed pressure drop. Additionally, as the superficial gas velocity increases, the amount of bed particles in the packing voids decreases, due to increased vertical segregation. This leads to further decreases in the bed pressure drop. The increased vertical segregation will also cause a decrease of the bed-to-tube heat transfer coefficient, at high superficial gas velocities, as the bed particles act as heat carriers inside the bed. If their number inside the packing voids decreases, so does the heat transfer ability of the bed.

5.1.4 Beneficial packing material parameters

The packing materials could be evaluated based on how they affect the maximum bubble size inside the bed, bed heat transfer ability, bed pressure drop and the vertical segregation of the bed.

The maximum bubble size, and the corresponding mass transfer rate, are not estimated in this thesis. However, by directly observing the size and structure of the packings, it would seem reasonable to assume that they would all be able to physically restrict the maximum bubble size in a bed to a size below that of the large bubbles that could be expected to form in deep beds in large-scale reactors. How the packings perform in comparison to each other would have to be evaluated in an experiment where the mass transfer rate between the gas and solid particle phase is measured.

Considering the heat transfer ability of the bed, the packings should have a high void ratio with an open structure, as not to hinder the movement of the bed particles through the bed. They should also not be able to cover a large portion of any heat exchange area they come into contact with, as any area they cover will be denied for bed particle heat exchange.

The packings should also have a high void ratio and open structure to avoid additional increases in bed pressure drop. The increased velocity and constricted pathways in the packing voids will lead to increased friction between the bed particles and the packing, increasing pressure drop.

To avoid having large quantities of bed material segregate at high superficial gas velocities, the packings should have a high void ratio. Otherwise, the increasing gas velocity inside the packing voids that comes with decreasing packing void ratio will expel more bed particles into the volume above the packings. A more closed structure could also reduce vertical segregation by containing a larger amount of bed material in the packing region, as seen when comparing the RMSR and Hiflow packings in figure 13. However, the closed structure will disadvantage the packed bed in other ways, as previously mentioned in this section.

5.2 Possible error sources

During the experimental determination of the bed-to-tube heat transfer coefficient, the water flow rate was found to vary a non-negligible amount (±2%) from the average value. As the water supply was connected to the main water system of the building, the water flow could experience significant momentary decreases in flow rate if the water usage temporarily increased in another part of the building. The decreased flow rate would also lead to a momentary increase of the temperature in the reactor outlet. Care was taken not to collect any data during these periods, but it remains as a possible source of error. When measuring the temperature of the water outlet of the reactor, the thermocouple had to be placed approximately 2 cm away from the reactor wall. The effect has previously been evaluated and the resulting temperature difference was deemed marginal [13].

The desired height of the beds at rest was 13 cm. The actual height of the bed once the fluidizing bed material and packing material had been inserted into the reactor could not be confirmed visually, as the reactor was made of steel. The required amounts of bed material and packing were determined by filling an equivalent volume, a cylindrical container with a similar diameter, with packing and bed material up to 13 cm and weighing the mass of each component. Deviations of the bed height, especially the height of the packing, would mostly impact the pressure drop measurements. The calculations regarding vertical segregation and the corresponding mass balance are based around the packing height of 13 cm.

As the reactor was at a lab-scale size, wall effects could be expected to have a significant impact. That is especially the case for the larger RSMR and Hiflow packings, whose diameters of 32 mm were only 2.5 times smaller than the reactor diameter of 77.92 mm. The reactor also contained the horizontal water tube across the middle of the reactors cross-section. Combined, these two factors could result in varying stacking configurations of the two packing materials when poured into the reactor.

5.3 Areas of interest for future research

The main reason for using packing material in fluidized beds is for their ability to limit bubble growth and improve gas-solid mass transfer. Future research could be conducted to assess how the packing materials evaluated in this thesis perform in that regard. An option would be performing heat transfer experiments using gaseous fuels and oxygen-carrying bed particles to estimate the effect of the added packing material.

The parts of the experiment that were dependent on the height of the packed region of the bed being correct, such as the vertical segregation of the bed and the bed pressure drop, could be repeated using equipment more suited for the purpose. For example, by performing a cold flow experiment in a transparent reactor.

None of the evaluated packing materials were designed for the purpose of preventing bubble growth, but rather for use in chemical industry processes [10]. While this thesis examined what packing material properties were beneficial or disadvantageous, work could be done to develop a more refined packing specifically made for usage in fluidized beds. These packings would need to be sufficiently proficient at restricting bubble size to improve mass transfer, while still being open structured, have a high void ratio and not cause additional bed pressure drop increases due to packing-particle interaction.

Additional areas of interest could include increasing the size of the reactor and the number, orientation and size of the tube containing the water flow.

6 Conclusions

The experimental work consisted of estimating the bed-to-tube heat transfer coefficients at high bed temperatures for a single horizontal tube immersed in a packed fluidized bed, in a laboratory scale reactor. Additional results concerning bed pressure drop and vertical segregation of packing and bed particle material were generated. Five different packing materials were evaluated; RSMR 25-3, Hiflow® ring 25-5 metal, 6 mm Raschig ring, 10 mm Raschig ring and ½" aluminium silicate balls. The following conclusions could be drawn:

- Heat transfer coefficients varied significantly (674-1298 W/(m^2K)) depending on the packing material, for bed temperatures from 400°C to 900°C and a superficial gas velocity of 0.20 m/s. However, all added packings resulted in a lower heat transfer coefficient than that of a bed containing no packing, when varying only the bed temperature.
- For all packings, varying the superficial gas velocity resulted in increasing heat transfer coefficients at lower velocities, followed by a maximum value and a slow decrease at higher velocities. The same trend is observed in fluidized beds with no packing.
- The pressure drop over the bed decreased when packing material was inserted into it, but varied greatly depending on the type of packing. The pressure drop decreased with increasing gas velocity, except for the ½" ASB at high velocities. Some packed beds experienced increased bed pressure drop due to bed particle-packing interaction.
- Vertical segregation of the packing and bed particle material increased with increasing superficial gas velocity, for all packing materials. The results varied greatly depending on the packing type.

- For the sake of the heat transfer ability of the bed, a packing material should have a high void ratio and an open structure as to not hinder bed particle movement inside the bed. A packing material should also not be able to significantly physically cover heat exchange surfaces, as the available area for bed particle heat exchange decreases.
- A packing material should also have an open structure and a high void ratio to minimize additional increases in bed pressure drop. Low void ratio packings will have higher fluidizing gas velocities in the packing voids, which together with a closed structure, will lead to higher bed pressure drop due to friction between the bed particles and the packing material.
- A high void ratio will also lead to low vertical segregation between the bed particles and the packing material, allowing for more bed material to remain the packing voids. Conversely, a low packing void ratio will lead to high gas velocities in the packing voids, that will expel more bed material into the volume above the packing, increasing the segregation.

Overall, to improve the mass transfer between a gas and a solid in a gas-solid reaction, like in the CLC process presented in the introduction, packing materials can be used with limited negative impact on the heat transfer process while decreasing the bed pressure drop. The chosen packing material should have a high void ratio and an open structure, while not physically covering heat exchange surfaces to a high degree. Out of the evaluated packings, the RMSR packing best exemplified these preferences, which corresponded well with its good performance seen in the experimental results.

References

[1] Blok, K., Williams, R., Katofsky, R. & Hendriks, C., "Hydrogen production from natural gas, sequestration of recovered CO_2 in depleted gas wells and enhanced natural gas recovery.", *energy*, 22, 1997

[2] Riemer, P., "Greenhouse gas mitigation technologies. An overview of the CO2 capture, storage and future activities of the IEA greenhouse gas R&D programme.", *The IEA Greenhouse Gas R&D Programme*, 1998

[3] Lyngfelt, A., & Leckner, B., "Technologies for CO2 separation. In: A. Lyngfelt, C. Azar (Eds.), *Minisymposium on CO2 capture and storage* (pp. 25 –35). Chalmers University of Technology and University of Gothenburg, Gothenburg, October 22.

[4] Lyngfelt, A., Leckner, B. & Mattison T., "A fluidized-bed combustion process with inherent CO_2 separation: application of chemical-looping combustion", *Chemical Engineering Science*, 56, 2001

[5] Stenberg, V., Rydén, M., Mattison, T. & Lyngfelt, A., "Exploring novel hydrogen production processes by integration of steam methane reforming with chemical-looping combustion (CLC-SMR) and oxygen carrier aided combustion (OCAC-SMR)", *International Journal of Greenhouse Gas Control*, 74, 2018

[6] Lyngfelt, A., Brink, A., Langorgen, O., Mattisson, T., Rydén, M. & Linderholm, C., "11,000 h of chemical-looping combustion operation—Where are we and where do we want to go?", *International Journal of Greenhouse Gas Control*, 88, 2019

[7] Kunii, D. & Levenspiel, O. "Fluidization Engineering. 2nd Edition", Stoneham, Massachusetts, USA, Butterworth-Heinemann, 1991.

[8] Aronsson, J., Pallarès, D., Rydén, M. & Lyngfelt, A., "Increasing Gas–Solids Mass Transfer in Fluidized Beds by Application of Confined Fluidization—A Feasibility Study", *Applied Sciences*, 9, 2018

[9] Aronsson, J., Krymarys, E., Stenberg, V., Mattison, T., Lyngfelt, A. & Rydén, M., "Improved Gas−Solids Mass Transfer in Fluidized Beds: Confined Fluidization in Chemical-Looping Combustion", *Energy & Fuels*, 33, 2019

[10] Basu, P., "Combustion and Gasification in Fluidized Beds, 1st Edition", Boca Raton, Florida, USA, CRC Press, 2006

[11] Mickley, H.S. & Fairbanks, D.F., "Mechanism of heat transfer to fluidized beds.", *AIChe Journal*, 1, 1955

[12] Sköldberg, V. & Öhrby, L., "Determination of heat transfer coefficient to tube submerged in bubbling fluidized bed reactor", Chalmers University of Technology, Gothenburg, Sweden, 2018

[13] Stenberg, V., Sköldberg, V., Öhrby, L. & Rydén, M., " Evaluation of bed-to-tube surface heat transfer coefficient for a horizontal tube in bubbling fluidized bed at high temperature", *Powder Technology*, 352, 2019

[14] Chiba, T. & Kobayashi, H., "Gas exchange between the bubble and emulsion phases in gas-solid fluidized beds", *Chemical Engineering Science*, 25, 1970

[15] Green, D., Perry, R., "Perry's Chemical Engineers' Handbook. 8th Edition", New York, McGraw-Hill, 2008

[16] Sutherland, J.P., Vassilatos, G., Kubota, H. & Osberg, G.L., ”The effect of packing on a fluidized bed”, *AIChe Journal*, 9, 1963

[17] Donsì, G. & Ferrari, G., “Expansion behaviour of confined fluidized beds of fine particles”, *The Canadian Journal of Chemical Engineering*, 67, 1989

[18] Welty, J., Wicks, C., Wilson, R., & Rorrer, G., Fundamentals of Momentum, Heat and Mass Transfer, 5th ed., Hoboken, N.J., USA, Wiley, 2005

[19] Sinnott, R.K., Coulson, J.M., & Richardson, J.F., Coulson and Richardson’s Chemical Engineering Volume 6 – Chemical Engineering Design, 4th ed., San Diego, CA, USA, Butterworth-Heinemann, 2005

[20] Metals S. Inconel alloy 600 [Cited 2020-01-06]. Available from: http://www.specialmetals.com/assets/smc/documents/alloys/inconel/inconel-alloy-600.pdf.

Appendix

Graphs of measured pressure drop over bed for all cases

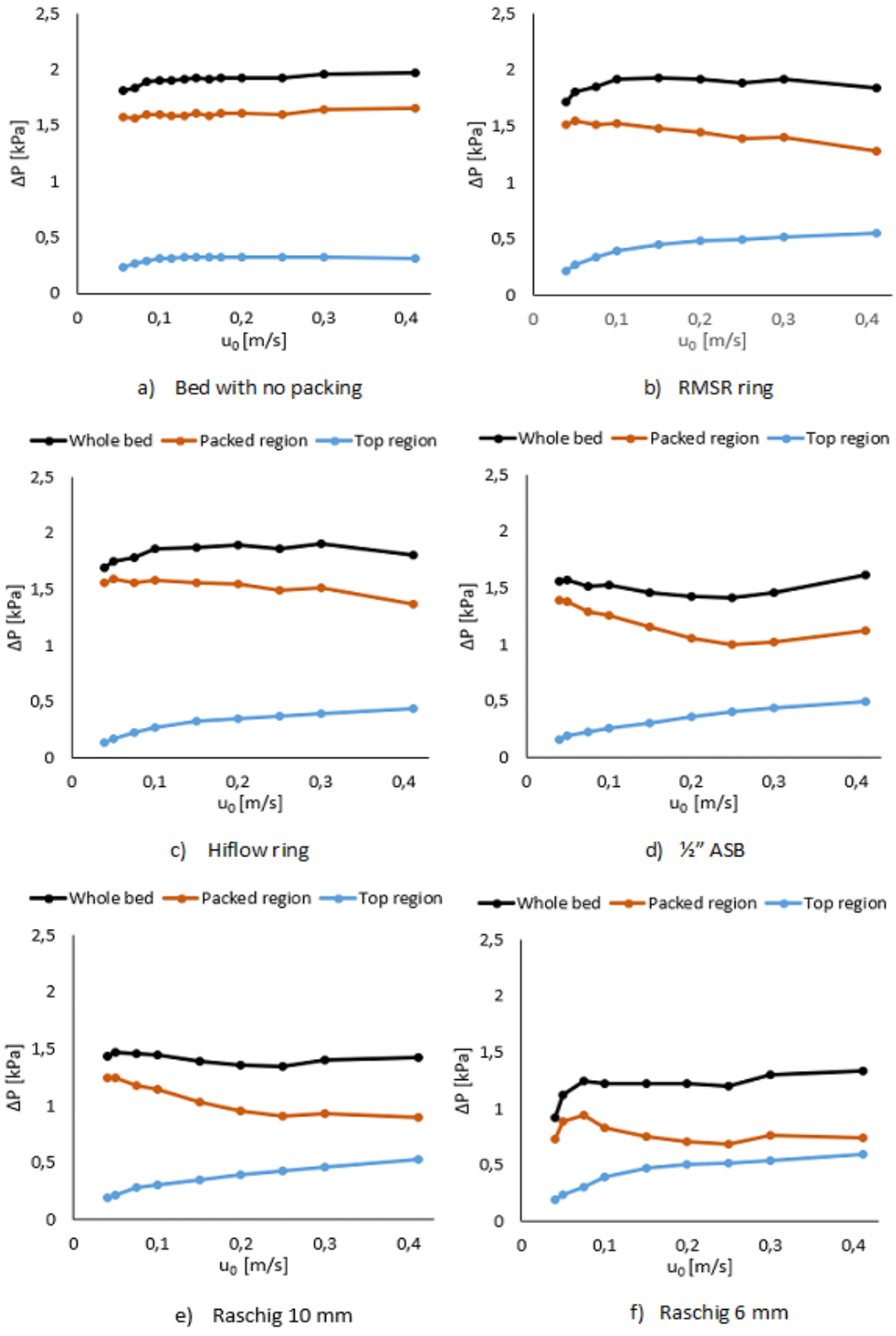

Figure 14: The measured pressure drop over whole bed, the packed region and the top region, for the five evaluated packings and the reference case.